IET Generation, Transmission & Distribution

Research Article

IET Journals
The Institution of Engineering and Technology

Comprehensive small-signal model and stability analysis of VSC-based medium-voltage DC distribution system

ISSN 1751-8687
Received on 28th April 2019
Revised 27th July 2019
Accepted on 27th August 2019
doi: 10.1049/iet-gtd.2019.0642
www.ietdl.org

Hanwen Gu[1], Zaibin Jiao[1] ✉

[1]*Shaanxi Key Laboratory of Smart Grid, Xi'an Jiaotong University, Xi'an, People's Republic of China*

✉ *E-mail: jiaozaibin@mail.xjtu.edu.cn*

Abstract: DC distribution technology is emerging as a prospective form of future power system owing to its advantages such as high controllability and easy compatibility. In medium- or low-voltage DC distribution systems, the two-level voltage-source converter (VSC) has become one of the preferred topologies for grid-connected converters. A comprehensive small-signal model for VSC-based DC distribution systems, which takes into consideration the AC filter, DC distribution cables, and all the controllers in the VSC is presented in this study. Based on the ideal AC source, an absolutely stable synchronous rotating coordinate system is built to preclude the influence of the short circuit ratio of the AC system. The proposed model is verified using a detailed electromagnetic transient simulation carried out using power systems computer-aided design (PSCAD). To analyse the impact of neglecting the AC filter and phase-locked loop controller, two simplified models are established, and a detailed comparison of the three models is presented. The results indicate that when using the two simplified models, the time-domain responses are significantly different from those in the PSCAD simulation and the obtained feasible domains of the control parameters tend to be either more optimistic or conservative. Thus, to carry out a small-signal stability analysis, the use of the proposed comprehensive model is recommended to ensure the safety of the DC distribution system.

1 Introduction

In recent years, DC distribution networks have been increasingly incorporated into electric power systems owing to their stronger controllability, easier compatibility, and lower power losses compared with the corresponding properties of AC distribution networks [1–4]. Considering that the voltage level of typical DC distribution networks does not exceed 100 kV, the two-level voltage-source converter (VSC) has become a widely used topology for grid-connected converters in DC distribution systems. Small-signal stability analysis is essential for the design and operation of a power system [5, 6], and thus, it is important to develop an accurate and efficient small-signal model for VSC-based DC distribution systems.

Small-signal modelling for DC system has been extensively studied in extant studies. In [7–11], small-signal models of VSC-based high voltage DC (VSC-HVDC) transmission systems were reported, and the impact of control parameters on small-signal stability was analysed. However, the AC filter was neglected in these models. Compared with the HVDC transmission system, the power quality requirement for AC systems is stricter in DC distribution systems. Furthermore, the presence of a two-level VSC converter with PWM modulation leads to the induction of a large number of harmonics into the AC system. Hence, ignoring the AC filter in small-signal models is inappropriate. A small-signal model of VSC-based DC distribution networks was established and a reduced-order method was proposed in [12]; however, this model neglected the phase-locked loop (PLL) controller to simplify the model. Although Zhou *et al*. [13] proved that the control parameters of the PLL controller do not considerably influence the small-signal stability, completely ignoring the PLL may cause the model to neglect some state variables and thereby inaccurately reflect the dynamic process of the system. In [14, 15], *dq* coordinate systems based on the point of common coupling (PCC) voltage were developed to propose small-signal models of VSC converters. The premise of these models was that the short circuit ratio (SCR) of AC systems is large and the perturbation of the PCC voltage can thus be neglected. However, AC systems in DC distribution networks are frequently weak, and hence, this modelling method is not suitable for DC distribution systems. In summary, the small-signal models established in earlier works pertained mainly to HVDC transmission systems and the controllers in VSC were simplified. A comprehensive small-signal model for a DC distribution network and the comparison of simplified and comprehensive models to verify the applicability of simplified models have not reported yet.

This study involved the development of a comprehensive small-signal model for VSC-based DC distribution systems, which represents the dynamics of the AC filter, DC distribution cables, and all the controllers in the VSC. Considering the impact of the SCR of an AC system, an absolutely stable *dq* coordinate system was established based on an ideal AC source. In addition, the proposed model was validated using a detailed electromagnetic transient simulation carried out using power system computer-aided design (PSCAD). Two simplified models that neglected the AC filter or PLL controller were also built and a detailed comparison of the three models was carried out to verify the applicability of the simplified models. The results indicated that when using the two simplified models, the obtained feasible domains of the control parameters tended to be either more optimistic or conservative, thereby leading to inaccurate stability results.

2 Power system and controllers under consideration

Fig. 1*a* shows the DC distribution network considered in this study. The AC system is connected to a medium-voltage DC distribution system via an interconnected transformer and a VSC station. In addition, an AC filter is introduced between the transformer and the VSC to enhance the power quality of the AC system. Fig. 1*b* shows the equivalent circuit of the system shown in Fig. 1*a*. The vertical impedance of the AC system (transformer and AC filter) can be represented in terms of R_1 and L_1, and C_g and R_{cg} represent the transverse capacitance and resistance of the AC filter, respectively. The VSC station is modelled using a phase reactor L_v and a DC capacitor C_v. In the DC distribution system, the DC cable is modelled as a π circuit consisting of r_{d1}, L_{d1} and C_{d1}, and R_L represents the DC load.

In this research, an ideal AC system is selected and its internal dynamics and controllers are neglected, as also performed in

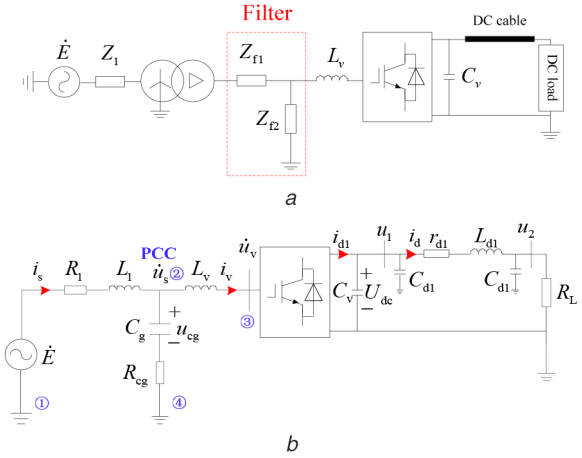

Fig. 1 *Considered DC distribution system*
(a) Structure of the considered DC distribution network, ***(b)*** Equivalent circuit of the considered system

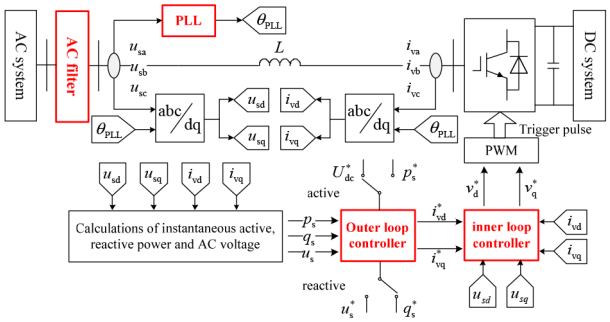

Fig. 2 *Control system of VSC converter*

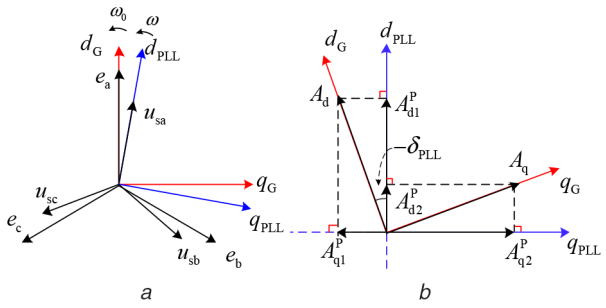

Fig. 3 *Transformation between d two different dq coordinate systems*
(a) Two different dq coordinate systems, ***(b)*** Transformation between $d_{\mathrm{G}}q_{\mathrm{G}}$ and $d_{\mathrm{PLL}}q_{\mathrm{PLL}}$ coordinate systems

related studies [6–12]. The control system of the VSC station can be represented as in Fig. 2. The PLL controller uses a control method similar to that used in [10] to synchronise the VSC station and the PCC voltage. The conventional vector-current controller (VCC) consisting of an outer and inner loop controller is adopted for active and reactive type control [8].

3 Non-linear state-space model of the DC distribution system

3.1 Selection of dq axis and coordinate transformation formula

In earlier studies, $d_{\mathrm{PLL}}q_{\mathrm{PLL}}$ coordinate systems based on the PCC voltage $\dot{u}_{\mathrm{s}}$, as shown in Fig. 3*a*, were established for small-signal modelling. The premise of this method was that the SCR of an AC system is large and the angular velocity of u_{s} is constant. When the perturbation of u_{s} cannot be neglected, the small-signal model established considering the $d_{\mathrm{PLL}}q_{\mathrm{PLL}}$ coordinate system is inaccurate. Considering the characteristics of the DC distribution system, this paper proposes an absolutely stable $d_{\mathrm{G}}q_{\mathrm{G}}$ coordinate system based on an ideal AC source. The d_{G} axis and the ideal AC source e_{a} are coincident, and hence the $d_{\mathrm{G}}q_{\mathrm{G}}$ component of the ideal AC source are $e_d = e$ and $e_q = 0$.

The VSC station maintains synchronicity with the PCC voltage via the PLL controller; thus, the electrical quantities in the VSC station undergo dq transformation under the $d_{\mathrm{PLL}}q_{\mathrm{PLL}}$ coordinate system. Fig. 3*b* shows the transformation relationship between the $d_{\mathrm{G}}q_{\mathrm{G}}$ and $d_{\mathrm{PLL}}q_{\mathrm{PLL}}$ axes. The coordinate transformation formula can be expressed as

$$\begin{cases} A_d^{\mathrm{P}} = A_{d1}^{\mathrm{P}} + A_{d2}^{\mathrm{P}} = A_d\cos\delta_{\mathrm{PLL}} - A_q sin\delta_{\mathrm{PLL}} \\ A_q^{\mathrm{P}} = -A_{q1}^{\mathrm{P}} + A_{q2}^{\mathrm{P}} = A_d\sin\delta_{\mathrm{PLL}} + A_q\cos\delta_{\mathrm{PLL}} \end{cases} \quad \begin{cases} A_d = A_{d1} - A_{d2} = A_d^{\mathrm{P}}\cos\delta_{\mathrm{PLL}} + A_q^{\mathrm{P}} sin\delta_{\mathrm{PLL}} \\ A_q = A_{q1} + A_{q2} = -A_d^{\mathrm{P}}\sin\delta_{\mathrm{PLL}} + A_q^{\mathrm{P}}\cos\delta_{\mathrm{PLL}} \end{cases} \tag{1}$$

where A and A^{P} represent the electrical quantities under $d_{\mathrm{G}}q_{\mathrm{G}}$ and $d_{\mathrm{PLL}}q_{\mathrm{PLL}}$ axes, respectively; angle between d_{G} axis and a-axis is $\theta_{\mathrm{G}} = \omega_0 t$, and angle between d_{PLL} axis and a-axis is $\theta_{\mathrm{PLL}} = \delta_{\mathrm{PLL}} + \omega_0 t$.

3.2 Modelling of AC network connected with VSC station

As shown in Fig. 1*b*, the differential equation obtained from branches ①②, ②③, and ②④ in the AC network can be expressed in $d_{\mathrm{G}}q_{\mathrm{G}}$ reference frame, as sequentially given in the following equation:

$$\begin{cases} L_1\dfrac{\mathrm{d}}{\mathrm{d}t}\begin{bmatrix} i_{sd} \\ i_{sq} \end{bmatrix} = -R_1\begin{bmatrix} i_{sd} \\ i_{sq} \end{bmatrix} + \omega_0 L_1\begin{bmatrix} i_{sq} \\ -i_{sd} \end{bmatrix} - \begin{bmatrix} u_{sd} \\ u_{sq} \end{bmatrix} + \begin{bmatrix} e \\ 0 \end{bmatrix} \\ L_{\mathrm{v}}\dfrac{\mathrm{d}}{\mathrm{d}t}\begin{bmatrix} i_{vd} \\ i_{vq} \end{bmatrix} = \omega_0 L_{\mathrm{v}}\begin{bmatrix} i_{vq} \\ -i_{vd} \end{bmatrix} + \begin{bmatrix} u_{sd} \\ u_{sq} \end{bmatrix} - \begin{bmatrix} u_{vd} \\ u_{vq} \end{bmatrix} \\ C_{\mathrm{g}}\dfrac{\mathrm{d}}{\mathrm{d}t}\begin{bmatrix} u_{\mathrm{cg}d} \\ u_{\mathrm{cg}q} \end{bmatrix} = \dfrac{1}{R_{\mathrm{cg}}}\begin{bmatrix} u_{sd} \\ u_{sq} \end{bmatrix} - \dfrac{1}{R_{\mathrm{cg}}}\begin{bmatrix} u_{\mathrm{cg}d} \\ u_{\mathrm{cg}q} \end{bmatrix} + \omega_0 C_{\mathrm{g}}\begin{bmatrix} u_{\mathrm{cg}q} \\ -u_{\mathrm{cg}d} \end{bmatrix} \end{cases} \tag{2}$$

where i_{sd}, i_{sq}, i_{vd}, i_{vq}, $u_{\mathrm{cg}d}$, and $u_{\mathrm{cg}q}$ are the introduced state variables. To eliminate u_{sd} and u_{sq}, the KCL algebraic equation pertaining to node ② can be expressed as

$$\begin{bmatrix} u_{sd} \\ u_{sq} \end{bmatrix} = R_{\mathrm{cg}}\begin{bmatrix} i_{sd} \\ i_{sq} \end{bmatrix} - R_{\mathrm{cg}}\begin{bmatrix} i_{vd} \\ i_{vq} \end{bmatrix} + \begin{bmatrix} u_{\mathrm{cg}d} \\ u_{\mathrm{cg}q} \end{bmatrix} \tag{3}$$

The intermediate variables u_{vd} and u_{vq} are eliminated as indicated in the subsequent sections.

3.3 Modelling of the VSC

3.3.1 Modelling of PLL controller of VSC: Fig. 4 shows the control block diagram of a typical PLL controller, in which the difference between u_{sq}^{P} and its reference 0 is provided as the input of the PI controller. When the PLL is in the steady-state, the d_{PLL} axis is synchronised to the PCC voltage u_{sa}, and the output is the phase angle θ_{PLL} of the d_{PLL}-axis.

The equation of the PLL controller considering the diagram shown in Fig. 4 can be expressed as

$$\theta_{PLL} = \int \left[-\left(k_p + \frac{k_i}{s} \right) \cdot u_{sq}^{P} + \omega_0 \right] dt \tag{4}$$

where k_p and k_i are the PI control parameters in the PLL controller. The derivative of (4) can be expressed as

$$\frac{d\delta_{PLL}}{dt} = -\left(k_p + \frac{k_i}{s} \right) \cdot u_{sq}^{P} \tag{5}$$

Then, the state-space equations of the PLL controller can be expressed as

$$\begin{cases} \dfrac{dz_1}{dt} = -u_{sq}^{P} \\ \dfrac{d\delta_{PLL}}{dt} = -k_p u_{sq}^{P} + k_i z \end{cases} \tag{6}$$

where $z_1$and δ_{PLL} are the introduced state variables. In addition, z_1 is an auxiliary variable representing the integral part of the PI controller in the PLL.

3.3.2 Modelling of VCC of VSC: Fig. 5 shows the control block diagram of the VCC in the VSC station consisting of the outer and inner loops. The active outer loop is responsible for the regulation of the DC voltage or active power, and the reactive outer loop maintains the AC voltage or reactive power at a constant value. The outputs obtained by the outer loops are provided as the input of the decoupled inner loops, which generate the d and q axes voltage reference for the PWM modulation.

The algebraic equations of the active outer loop can be expressed as (7) and (8)

$$i_{vd}^{P*} = (U_{dc}^{*} - U_{dc}) \left(k_{p1} + \frac{k_{i1}}{s} \right) \tag{7}$$

$$\begin{cases} P = \dfrac{3}{2}(u_{sd} i_{vd} + u_{sq} i_{vq}) \\ i_{vd}^{P*} = (P^{*} - P) \left(k_{p1} + \dfrac{k_{i1}}{s} \right) \end{cases} \tag{8}$$

where P and P* are the actual and reference values of the active power injected into the VSC station from the AC system, respectively, U_{dc} and U_{dc}^{*} are the actual and reference values of the DC voltage, respectively, and k_{p1} and k_{i1} are the PI control parameters in the active outer loop, respectively.

Similarly, the dynamic equations for the reactive outer loop can be expressed as (9) and (10)

$$\begin{cases} Q = \dfrac{3}{2}(-u_{sd} i_{vq} + u_{sq} i_{vd}) \\ i_{vq}^{P*} = (Q^{*} - Q) \left(k_{p2} + \dfrac{k_{i2}}{s} \right) \end{cases} \tag{9}$$

$$\begin{cases} u_s = \sqrt{u_{sd}^2 + u_{sq}^2} \\ i_{vq}^{P*} = (u_s^{*} - u_s) \left(k_{p2} + \dfrac{k_{i2}}{s} \right) \end{cases} \tag{10}$$

where Q and Q* are the actual and reference values of the reactive power injected into the VSC station from the AC system, respectively, u_s and u_s* are the actual and reference values of the AC voltage, respectively, and k_{p2} and k_{i2} are the PI control parameters in the reactive outer loop, respectively.

The d and q axes voltage reference from the inner loops can be expressed as

$$\begin{cases} \dfrac{dz_2}{dt} = -U_{dc} + U_{dc}^{*} / \dfrac{dz_2}{dt} = -P + P^{*} \\ \dfrac{dz_3}{dt} = -Q + Q^{*} / \dfrac{dz_3}{dt} = -u_s + u_s^{*} \\ \dfrac{dz_4}{dt} = i_{vd}^{P*} - i_{vd}^{P} \\ \dfrac{dz_5}{dt} = i_{vq}^{P*} - i_{vq}^{P} \end{cases} \tag{11}$$

where z_2 and z_3, and z_4 and z_5, are the introduced state variables and auxiliary variables representing the integral part of the PI controllers in the VCC, respectively.

Note that u_{vd}^{P} and u_{vq}^{P} can be expressed using (7)–(11), which can eliminate the intermediate variables u_{vd} and u_{vq}.

3.4 Modelling of DC network connected with VSC station

The equivalent circuit of the DC network is shown in Fig. 6. The DC distribution line is modelled as a π circuit considering the fact that the cables are widely used in DC distribution systems. The DC load is represented by a resistance R_L.

Assuming that the active power loss in the VSC station is neglected, the dynamic equations of the DC network shown in Fig. 6 can be expressed as

$$\begin{cases} (C_v + C_{d1}) \dfrac{dU_{dc}}{dt} = i_{d1} - i_d \\ i_{d1} = \dfrac{3}{2} \cdot \dfrac{u_{sd} i_{vd} + u_{sq} i_{vq}}{U_{dc}} \\ L_{d1} \dfrac{di_d}{dt} = u_{dc} - u_L - i_d \\ C_{d1} \dfrac{du_L}{dt} = i_d - \dfrac{1}{R_L} u_L \end{cases} \tag{12}$$

where U_{dc}, i_d, and u_L are the introduced state variables, and i_{d1} is the intermediate variable.

4 Linearised small-signal model of the DC distribution system

4.1 Linearised small-signal model

A 15-order non-linear state-space model of the DC distribution system shown in Fig. 1 can be expressed based on the discussion in Section 3 as

$$\frac{d\boldsymbol{x}}{dt} = \boldsymbol{f}(\boldsymbol{x}, \boldsymbol{u}) \tag{13}$$

where the state vector $\boldsymbol{x}$ has an order of 15 and consists of 6 AC network variables (i_{sd}, i_{sq}, i_{vd}, i_{vq}, u_{cgd}, u_{cgq}), 2 PLL controller variables (z_1, δ_{PLL}), 4 VCC variables (z_2, z_3, z_4, z_5), and 3 DC network variables (U_{dc}, i_d, u_L). The input vector is $\boldsymbol{u} = [U_{dc}^{*}, Q^{*}]$.

To investigate the small-signal stability of VSC-based DC distribution system based on the first Lyapunov criterion, the linearised state-space equations can be obtained via

$$\frac{d\boldsymbol{\Delta x}}{dt} = \boldsymbol{A}\boldsymbol{\Delta x} + \boldsymbol{B}\boldsymbol{\Delta u} \tag{14}$$

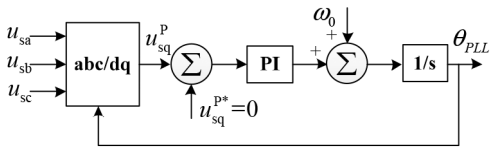

Fig. 4 *Control block diagram of the typical PLL controller*

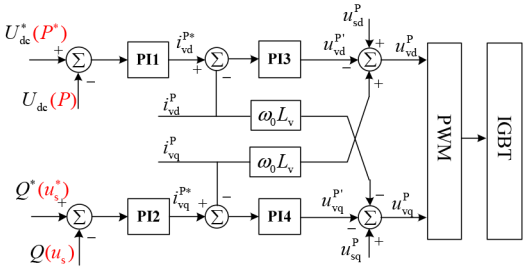

Fig. 5 *Control block diagram of the VCC in VSC station*

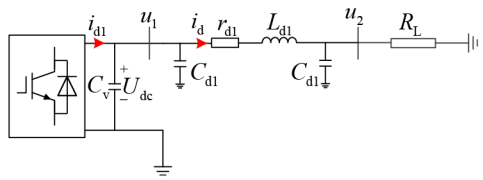

Fig. 6 *Equivalent circuit of the DC network connected with VSC converter*

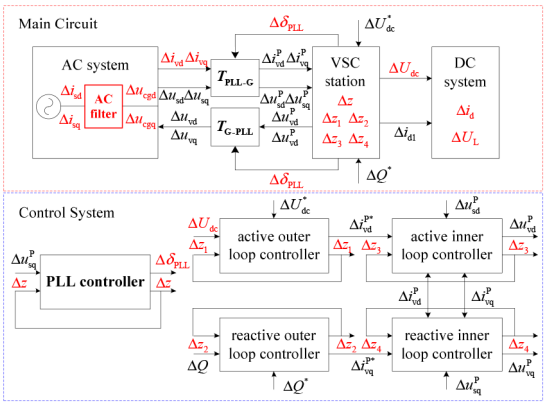

Fig. 7 *Relationship between submodels of VSC system*

where $\boldsymbol{A}$ and $\boldsymbol{B}$ are the characteristic matrix and the input matrix, respectively, and $\boldsymbol{\Delta x}$ and $\boldsymbol{\Delta u}$ denote the small-signal state vector and the input vector, respectively. Based on the first Lyapunov criterion, the small-signal stability of the DC distribution system can be analysed by considering the eigenvalues of the characteristic matrix $\boldsymbol{A}$. The block diagram of the small-signal model is shown in Fig. 7, and the variables between the different submodels are the interfaced variables. The state variables are labelled in red.

4.2 Verification and comparison of small-signal models

To verify the accuracy of (14), the aforementioned model (Model I) was analytically evaluated using a Matlab program. The actual DC distribution system model was simulated using PSCAD, and a Bergeron model is chosen for the DC distribution line to make the simulation program more realistic. The parameters of the system are listed in Table 1.

Initially, the operation points of the system are $U_{dc} = 1$ p.u. and $Q = 0$ p.u. The introduced small disturbance is a 0.1 kV step change of the DC voltage reference from 10 to 10.1 kV at 3 s. The curves of different state variables obtained using the two methods during the small disturbance are compared in Fig. 8.

The results shown in Fig. 8 illustrate that the time-domain responses of ΔU_{dc}, Δi_{vd}, Δi_{sd}, Δi_{sq}, Δu_{cgd} and Δu_{cgq} calculated using MATLAB closely coincide with those obtained using the simulation in PSCAD; this indicates the accuracy of the aforementioned small-signal model.

Table 1 System parameters [16]

Parameters	Values	
main circuit	AC system resistance R_1	0.2 Ω
	AC system inductance L_1	1 mH
	converter inductance L_v	10 mH
	filter capacitance C_g	2 μF
	filter resistance R_{cg}	2 Ω
	DC side capacitance C_v	4 mF
	DC line resistance R_{d1}	0.1 Ω
	DC line inductance L_{d1}	0.01 H
	DC line capacitance C_{d1}	5 μF
	resistive load	1000 Ω
control system	PLL controller (k_p, k_i)	(50, 900)
	DC voltage controller (k_{p1}, k_{i1})	(5, 10)
	reactive power controller (k_{p2}, k_{i2})	(0.05, 10)
	active inner controller (k_{p3}, k_{i3})	(5, 10)
	reactive inner controller (k_{p4}, k_{i4})	(5, 10)

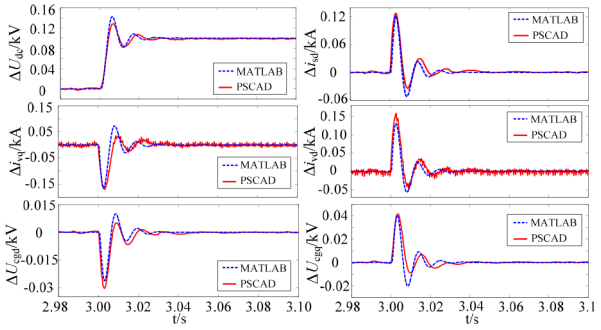

Fig. 8 *Responses of the state variables ΔU_{dc}, Δi_{vd}, Δi_{sd}, Δi_{sq}, Δu_{cgd} and Δu_{cgq} in Model I to the DC voltage reference disturbance*

To analyse the applicability of the simplified models, Model II (neglecting the AC filter) and Model III (neglecting the PLL controller in the VSC station) were established using the same method as that used for Model I. The comparison of the curves of the different state variables obtained using MATLAB and PSCAD during the 0.1 kV step change of the DC voltage reference at 3 s is presented in Fig. 9.

The results shown in Fig. 9 illustrate that the time-domain responses obtained using MATLAB and PSCAD are considerably different. Thus, the proposed model, that is, Model I can be considered to be more accurate than Models II and III, and it is concluded that neglecting the AC filter or PLL controller in the small-signal model can produce a significant error.

5 Small-signal stability analysis

5.1 Eigenvalue analysis

The eigenvalues of the characteristic matrix, along with the frequencies, damping ratios, and main participating variables for VSC-based DC distribution system shown in Fig. 1 are presented in Table 2. Note that only the main participating variables obtained by Model I are listed in Table 2.

The damping ratio [15] of an underdamped mode $\lambda = \sigma \pm j\omega$ can be expressed as

$$\xi = \frac{-\sigma}{\sqrt{\sigma^2 + \omega^2}} \tag{15}$$

When the damping ratio $\xi < 0.05$, the corresponding mode can be regarded as a poor-damping mode, which may give rise to a low-frequency oscillation and lead to system small-signal instability.

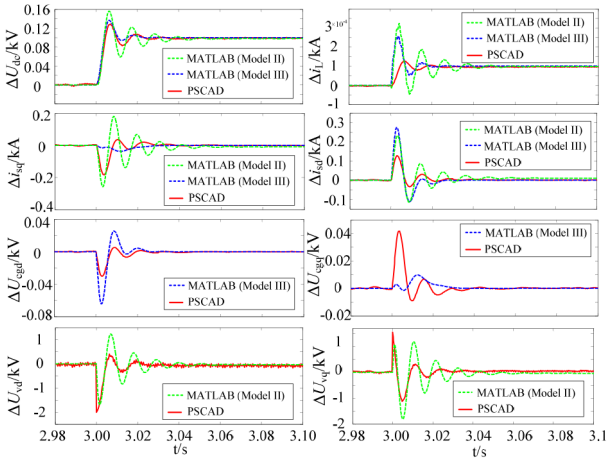

Fig. 9 *Responses of the state variables in Models II and III to DC voltage reference disturbance*

Table 2 Eigenvalue analysis for Model I (integrated model), Model II (without AC filter), and model III (without PLL controller)

Modes	Model I			Model II		Model III		Main participating variables for Model I
	Eigenvalue	*f*, Hz	*ξ*	Eigenvalue	*ξ*	Eigenvalue	*ξ*	
1	**−1.99**	**0**	**1**	**−2**	**1**	**−2**	**1**	$\Delta z_2\ \Delta z_3\ \Delta z_4\ \Delta z_5$
2	**−2±j0.004**	**0**	**1**	**−1.97±j0.07**	**1**	**−2±j0.004**	**1**	$\Delta z_4\ \Delta z_5$
3	−25.5±j16.7	2.66	0.84	**−24.4±j16.4**	**0.83**	—	—	$\underline{\Delta z_1\ \Delta\delta_{PLL}}$
4	−134.7	0	1	−186.6±j49	0.968	−157.7±j90	0.867	$\Delta i_{sd}\ \Delta i_{sq}\ \Delta z_3\ \Delta z_5$
5	−212.8	0	1					$\Delta i_{sd}\ \Delta i_{sq}\ \Delta z_3\ \Delta z_5$
6	**−105±j4474**	**712.1**	**0.02**	**−105±j4474**	**0.023**	**−105±j4474**	**0.023**	$\Delta i_d\ \Delta U_L$
7	−151±j570.9	90.86	0.26	−196.2±j550	0.336	−189±j528	0.337	$\Delta i_{sd}\ \Delta i_{sq}\ \Delta z_2\ \Delta z_3\ \Delta z_4$
8	***−251.5±j316***	***50.3***	***0.62***	***−43204.7***	***1***	−254±j309	0.636	$\boldsymbol{\Delta i_{sd}\ \Delta i_{sq}\ \Delta u_{cgd}\ \Delta u_{cgq}}$
9	***−2044±j258***	***41.11***	***0.99***	***−44894.1***	***1***	−2043±j325	0.987	$\boldsymbol{\Delta i_{sd}\ \Delta i_{sq}\ \Delta u_{cgd}\ \Delta u_{cgq}}$

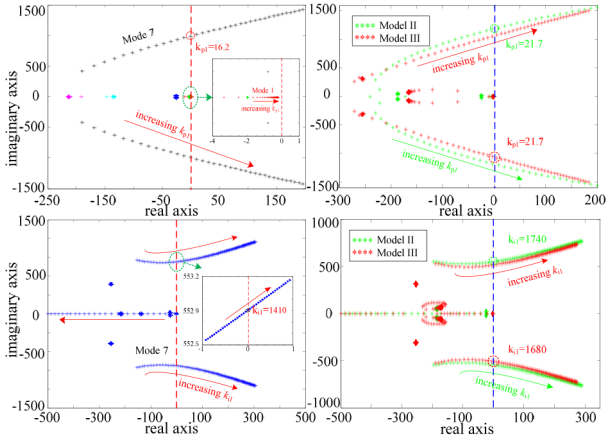

Fig. 10 *Eigenvalue locus of Models I, II, and III with changes in k_{p1} and k_{i1}*

(a) With change in k_{p1} of Model I, ***(b)*** With change in k_{p1} of Models II, III, ***(c)*** With change in k_{i1} of Model I, ***(d)*** With change in k_{i1} of Models II, III

Furthermore, the modes closer to the imaginary axis correspond to slower decays in the time domain, and they may change to appear in the right side of the imaginary axis owing to the error caused by system parameters and small-signal model. Two types of critical modes are in bold in Table 2.

The data presented in Table 2 indicate that when the AC filter is neglected, the state variables Δi_{sd}, Δi_{sq}, Δu_{cgd} and Δu_{cgq} are not introduced in Model II. The dynamics of mode 8 and mode 9 (labelled as bold italic) cannot be clarified because the variables that are neglected are the main participating variables of these modes in Model I. Similarly, the dynamics of mode 3 (labeled underlined) are ignored owing to the omission of Δz_1 and $\Delta\delta_{PLL}$. Hence, more oscillation modes emerge in the considered system when using Model I and neglecting the AC filter or PLL controller may weaken the small-signal stability problems of the DC distribution system.

5.2 Impact of control parameters of outer loop controller of VCC on small-signal stability

This section presents the analysis of the impact of the outer loop controller parameters k_{p1}, k_{i1}, k_{p2} and k_{i2} on the small-signal stability and the evaluation of the effect of neglecting the AC filter or PLL controller by comparing the eigenvalue loci and feasible regions of the control parameters.

Fig. 10 shows the eigenvalue loci involving the change in k_{p1} and k_{i1}, and the evaluation of the impact of the parameters on the dominate mode (mode 7) of the system using Models I, II, and III. Fig. 10 indicates that when k_{p1} varies from 1 to 50 or k_{i1} varies from 1 to 10,000, mode 7 gradually changes from an underdamped stable mode to a negatively damped unstable mode. Figs. 11*a* and *b* demonstrate the relationships among the parameters and the real axis, as obtained by the three models. Fig. 11*a* indicates that the

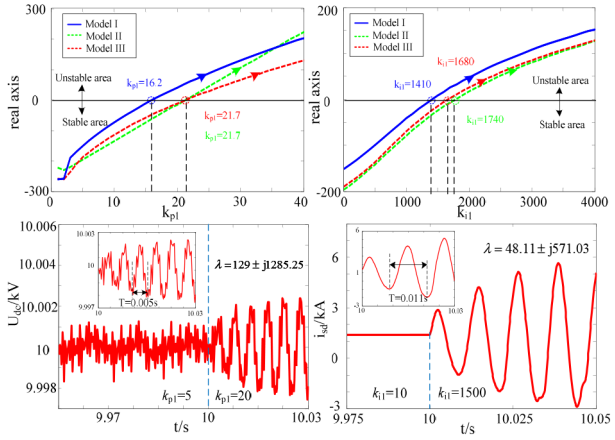

Fig. 11 *Feasible regions of k_{p1} and k_{i1} obtained using Models I, II, and III and variation curves in PSCAD*

(a) Relationship between k_{p1} and real axis, ***(b)*** Relationship between k_{i1} and real axis, ***(c)*** Variation curve of DC voltage when k_{p1} changes, ***(d)*** Variation curve of i_{sd} when k_{i1} changes

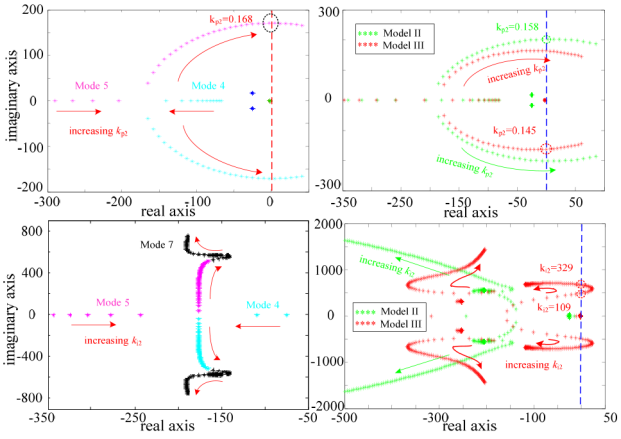

Fig. 12 *Eigenvalue locus of Models I, II, and III with changes in k_{p2} and k_{i2}*

(a) With change in k_{p2} of Model I, ***(b)*** With change in k_{p2} of Models II, III, ***(c)*** With change in k_{i2} of Model I, ***(d)*** With change in k_{i2} of Models II, III

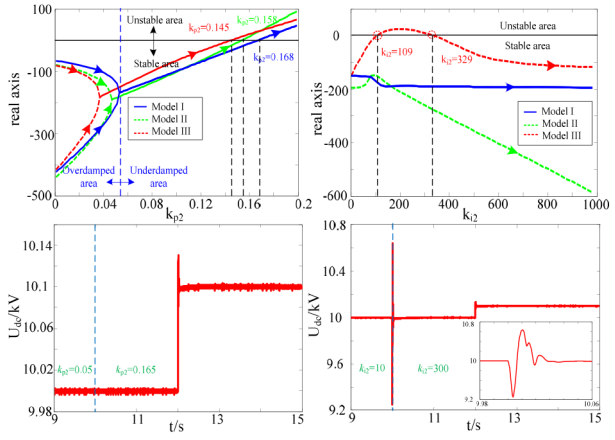

Fig. 13 *Feasible regions of k_{p2} and k_{i2} obtained using Models I, II, and III and variation curves in PSCAD*

(a) Relationship between k_{p2} and real axis, ***(b)*** Relationship between k_{i2} and real axis, ***(c)*** Variation curve of DC voltage when k_{p2} changes, ***(d)*** Variation curve of DC voltage when k_{i2} changes

feasible regions of k_{p1} obtained by the three models are $k_{p1} < 16.2$, $k_{p1} < 21.7$, and $k_{p1} < 21.7$. Similarly, Fig. 11*b* indicates that the feasible regions of k_{i1} are $k_{i1} < 1410$, $k_{i1} < 1740$, and $k_{i1} < 1680$ for the three models. To verify the eigenvalue analysis results, the time-domain responses of the DC distribution system simulated in PSCAD were plotted, as presented in Figs. 11*c* and *d*. Fig. 11*c* shows that when k_{p1} steps from 5 to 20 at 10 s, the DC voltage experiences an amplitude oscillation, which corroborates only with the stable region of $k_{p1} = 16.2$ obtained using Model I, as shown in Fig. 11*a*. Furthermore, the eigenvalues of the oscillatory mode (mode 7) pertaining to Model I are $\lambda = 129 \pm j1285.25$ and the period of amplitude oscillation is 0.005 s, which strongly agree with the results obtained using the PSCAD simulation. Similarly, Fig. 11*d* indicates that when k_{i1} steps from 10 to 1500, the AC current i_{sd} experiences an amplitude oscillation, which corroborates only with the stable region of $k_{i1} < 1410$ obtained using Model I. In addition, the period of amplitude oscillation is 0.011 s, which is in agreement with the PSCAD simulation results. The close agreements between the MATLAB-based eigenvalue analysis and simulation results obtained using PSCAD verify that Model I is more accurate than Models II and III, and the feasible regions of k_{p1} and k_{i1} obtained using Models II and III are too optimistic. In addition, Figs. 10*a* and *c* indicate that smaller values of k_{p1} and k_{i1} are preferable to realise small-signal stability.

In a comparable manner, Fig. 12 shows the eigenvalue loci with the change in k_{p2} and k_{i2}, pertaining to Models I, II, and III. Figs. 13*a* and *b* show the relationships among k_{p2}, k_{i2}, and the real axis obtained by the three models, and the feasible regions of k_{p2} and k_{i2} are $k_{p2} < 0.168$; $k_{p2} < 0.158$; $k_{p2} < 0.145$, $k_{i2} < 109$; or $k_{i2} > 329$. To verify the results, the time-domain responses of the DC voltage, simulated in PSCAD, were plotted, as presented in Figs. 13*c* and *d*. These figures indicate that when k_{p2} steps from 0.05 to 0.165 or when k_{i2} steps from 10 to 300, no small-signal instability appears in the system, which agrees only with the stable region of $k_{p2} < 0.168$ obtained in the case of Model I. This analysis demonstrates that Model I is more accurate than Models II and III, and the feasible regions of k_{p2} and k_{i2} obtained using Models II and III are too conservative.

5.3 Impact of control parameters of inner loop controller of VCC on small-signal stability

Fig. 14 shows the eigenvalue loci with changes in k_{p3} and k_{i3} and assists in the evaluation of the impact of the parameters on the dominant modes (mode 7) of the system, pertaining to Models I, II, and III. Fig. 14*a* indicates that when k_{p3} varies from 0.01 to 5, mode 7 changes gradually from a negatively damped unstable mode to an underdamped stable mode. Fig. 14*b* shows that when k_{i3} varies from 1 to 5000, mode 7 obtained using Models I and III changes from a stable mode to an unstable mode, whereas mode 7 obtained using Model II is continuously stable. Fig. 15 shows the relationships among k_{p3}, k_{i3}, and the real axis obtained using the three models, and the feasible regions of k_{p3} and k_{i3} are $k_{p3} > 0.41$, $k_{i3} < 3495$; $k_{p3} > 0.22$; $k_{p3} > 0.6$, and $k_{i3} < 3690$. Furthermore, Fig. 14 indicates that a larger value of k_{p3} and smaller value of k_{i3} are preferable to ensure small-signal stability.

Similarly, the findings shown in Fig. 16 were used to evaluate the impact of k_{p4} and k_{i4} on the dominant modes (mode 4 and mode 5) of the system, pertaining to Models I, II, and III. Fig. 16*a* indicates that when k_{p4} varies from 0.01 to 10, mode 4 and mode 5 gradually change from unstable negatively damped modes to stable underdamped modes, and finally, they become overdamped modes. Fig. 16*b* shows that when k_{i4} varies from 1 to 1000, mode 4 and mode 5 are continuously stable. Fig. 17 shows the relationships among k_{p4}, k_{i4}, and the real axis as obtained by the three models, and the feasible regions of k_{p4} and k_{i4} are noted to be $k_{p4} > 0.325$, $k_{p4} > 0.321$, and $k_{p4} > 0.348$.

5.4 Impact of control parameters of PLL controller on small-signal stability

The impact of k_p and k_i on small-signal stability cannot be analysed using Model III because the PLL controller is ignored in this case.

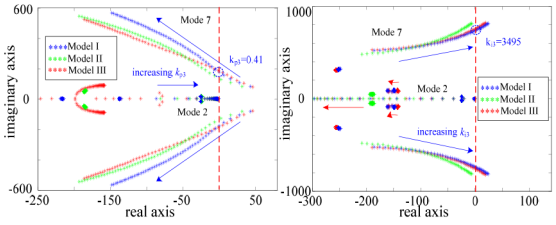

Fig. 14 *Eigenvalue locus of Models I, II, and III with the changes in k_{p3} and k_{i3}*

(a) With change in k_{p3} of Models I, II, and III, ***(b)*** With change in k_{i3} of Models I, II, and III

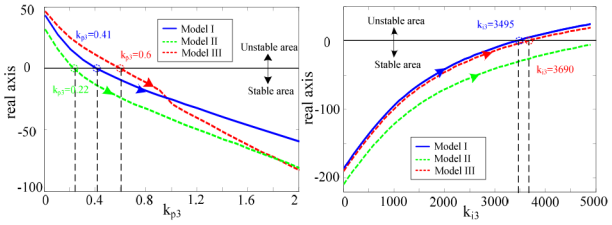

Fig. 15 *Feasible regions of k_{p3} and k_{i3} obtained using Models I, II, and III*

(a) Relationship between k_{p3} and real axis, ***(b)*** Relationship between k_{i3} and real axis

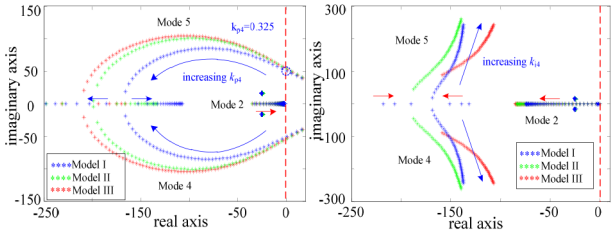

Fig. 16 *Eigenvalue locus of Models I, II, and III with the changes in k_{p4} and k_{i4}*

(a) With change in k_{p4} of Models I, II, and III, ***(b)*** With change in k_{i4} of Models I, II, and III

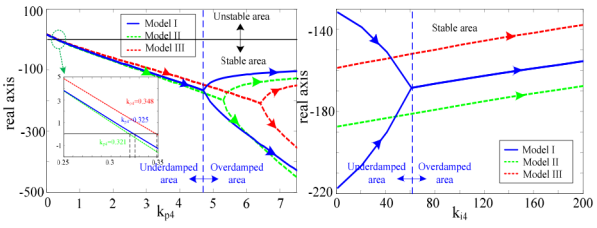

Fig. 17 *Feasible regions of k_{p4} and ki4 obtained using Models I, II, and III*

(a) Relationship between k_{p4} and real axis, ***(b)*** Relationship between k_{i4} and real axis

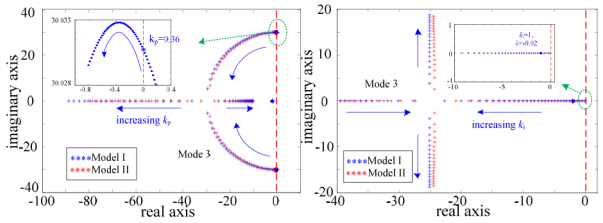

Fig. 18 *Eigenvalue locus of Models I, II, and III with changes in k_p and k_i*

(a) With change in k_p of Models I, II, and III, ***(b)*** With change in k_i of Models I, II, and III

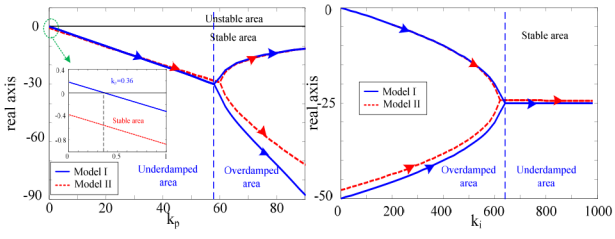

Fig. 19 *Feasible regions of k_p and k_i obtained using Models I, II, and III*

(a) Relationship between k_p and real axis, ***(b)*** Relationship between k_i and real axis

Accordingly, this part discusses the analysis of the impact of k_p and k_i on small-signal stability by considering Models I and II.

Fig. 18 shows the eigenvalue loci with changes in k_p and k_i and assists in evaluating the impact of the parameters on the dominate modes (mode 3) of the system pertaining to Models I and II. Fig. 18*a* shows that when k_p varies from 0.01 to 100, mode 3 obtained by Model I changes from an unstable mode to a stable mode, whereas mode 3 obtained using Model II is continuously stable. Fig. 18*b* shows that when k_i varies from 1 to 1000, mode 3 changes gradually from an overdamped stable mode to an underdamped stable mode. Fig. 19 shows the relationships among k_p, k_i, and the real axis, and the feasible region of k_p and k_i obtained using Model I is $k_p > 0.36$. Further, in the case of Model II, the system is continuously small-signal stable with changes in k_p and k_i.

Table 3 shows the effect of neglecting the AC filter (Model II) or PLL controller (Model III) on the feasible regions of the control parameters in the VSC station. It can be concluded that using simplified small-signal models potentially leads to the determination of optimistic or conservative feasible regions of control parameters in the VSC station, thereby leading to inaccurate small-signal stability conclusions.

6 Conclusion

This paper proposed a comprehensive small-signal model of a VSC-based DC distribution system, which considers the AC filter, DC distribution cables, and all the controllers in the VSC station. Based on the ideal AC source, an absolutely stable synchronous rotating coordinate system was established to avoid the influence of the SCR of the AC system. To analyse the effect of ignoring AC filter and PLL controller, two simplified models were also established and a detailed comparison of the three models was performed. The primary conclusions of this study can be listed as follows:

(i) By comparing the time-domain responses of different state variables, obtained by MATLAB and PSCAD, it can be concluded that the proposed comprehensive model is more accurate than the other considered models, and neglecting the AC filter or PLL controller in the small-signal model may produce a significant error.

(ii) The eigenvalue analysis indicated that more oscillation modes appear in the DC distribution system when using the comprehensive model, and thus, neglecting the AC filter or PLL controller may weaken the small-signal stability problems of the DC distribution system.

(iii) Table 3 indicates that using simplified small-signal models potentially leads to the determination of optimistic or conservative feasible regions of the control parameters in the VSC station, which may lead to incorrect small-signal stability conclusions.

(iv) The eigenvalue loci pertaining to the change in the control parameters in the VSC station indicate that to ensure small-signal stability, it is preferable to choose smaller values of PI control parameters of the DC voltage outer loop controller (k_{p1}, k_{i1}), larger values of the proportional parameters of the active inner loop controller (k_{p3}), and smaller values of the integral parameters of the active inner loop controller (k_{i3}). Both underdamped and overdamped modes emerged in the eigenvalue loci with changes in the other control parameters (k_{p2}, k_{i2}, k_{p4}, k_{i4}, k_p, k_i); therefore, the values of these parameters must be suitably selected according to the actual condition of the system.

Table 3 Impact of ignoring the AC filter and PLL controller on the feasible domain of the control parameters

Parameters		Model I	Model II(without AC filter)	Impact	Model III(without PLL controller)	Impact
DC voltage controller	k_{p1}	k_{p1}<16.2	k_{p1}<21.7	optimistic	k_{p1}<21.7	optimistic
	k_{i1}	k_{i1}<1410	k_{i1}<1740	optimistic	k_{i1}<1680	optimistic
reactive power controller	k_{p2}	k_{p2}<0.168	k_{p2}<0.158	conservative	k_{p2}<0.145	conservative
	k_{i2}	k_{i2}-	k_{i2}-	no impact	k_{i2}<109 or k_{i2}>329	conservative
active inner controller	k_{p3}	k_{p3}>0.41	k_{p3}>0.22	optimistic	k_{p3}>0.6	conservative
	k_{i3}	k_{i3}<3495	k_{i3}-	optimistic	k_{i3}<3690	optimistic
reactive inner controller	k_{p4}	k_{p4}>0.325	k_{p4}>0.321	optimistic	k_{p4}>0.348	conservative
	k_{i4}	k_{i4}-	k_{i4}-	no impact	k_{i4}-	no impact
PLL controller	k_p	k_p>0.36	k_p-	optimistic	—	—
	k_i	k_i-	k_i-	no impact	—	—

7 References

[1] Saeedifard, M., Iravani, R.: 'Dynamic performance of a modular multilevel back-to-back HVDC system', *IEEE Trans. Power Deliv.*, 2010, **25**, (4), pp. 2903–2912

[2] Wang, Y., Song, Q., Zhao, B., *et al.*: 'Quasi-square-wave modulation of modular multilevel high-frequency DC converter for medium-voltage DC distribution application', *IEEE Trans. Power Electron.*, 2017, **33**, (9), pp. 7480–7495

[3] Anderson, B.R., Xu, L., Horton, P.J., *et al.*: 'Topologies for VSC transmission', *Power Eng. J.*, 2002, **16**, (3), pp. 142–150

[4] Flourentzou, N., Agelidis, V.G., Demetriades, G.D.: 'VSC-based HVDC power transmission systems: an overview', *IEEE Trans. Power Electron.*, 2009, **24**, (3), pp. 592–602

[5] Karawita, C., Annakkage, U.D.: 'Multi-infeed HVDC interaction studies using small-signal stability assessment', *IEEE Trans. Power Deliv.*, 2009, **24**, (2), pp. 910–918

[6] Osauskas, C., Wood, A.: 'Small-signal dynamic modeling of HVDC systems', *IEEE Trans. Power Deliv.*, 2003, **18**, (1), pp. 220–225

[7] Pinares, G., Bongiorno, M.: 'Modeling and analysis of VSC-based HVDC systems for DC network stability studies', *IEEE Trans. Power Deliv.*, 2015, **31**, (2), pp. 848–856

[8] Kalcon, G.O., Adam, G.P., Anaya-Lara, O., *et al.*: 'Small-signal stability analysis of multi-terminal VSC-based DC transmission systems', *IEEE Trans. Power Syst.*, 2012, **27**, (4), pp. 1818–1830

[9] Pinares, G., Tjernberg, L.B., Breitholtz, C., *et al.*: 'On the analysis of the dc dynamics of multi-terminal VSC-HVDC systems using small signal modeling'. 2013 IEEE Grenoble Conf., Grenoble, France, June 2013

[10] Xiong, L., Han, M., Yao, S.: 'Influence of PLL on the stability analysis of VSC-MTDC and parameter selection', *Trans. China Electrotech. Soc.*, 2015, **30**, (16), pp. 203–212

[11] Alsseid, A.M., Jovcic, D., Starkey, A.: 'Small signal modelling and stability analysis of multiterminal VSC-HVDC'. 2011 14th European Conf. on Power Electronics and Applications, Birmingham, UK, August 2011

[12] Jia, Q., Yan, G., Cai, Y., *et al.*: 'Small-signal stability analysis of photovoltaic generation connected to weak AC grid', *Journal of Modern Power Systems and Clean Energy*, 2019, **7**, (2), pp. 254–267

[13] Zhou, J.Z., Ding, H., Fan, S., *et al.*: 'Impact of short circuit ratio and phase locked loop parameters on the small-signal behaviour of a VSC-HVDC converter', *IEEE Trans. Power Deliv.*, 2014, **29**, (5), pp. 2287–2296

[14] Mortazavian, S., Shabestary, M.M., Mohamed, Y.A. R.I.: 'Analysis and dynamic performance improvement of grid-connected voltage–source converters under unbalanced network conditions', *IEEE Trans. Power Electron.*, 2016, **32**, (10), pp. 8134–8149

[15] Guo, C., Yang, J., Zhao, C.: 'Investigation of small-signal dynamics of modular multilevel converter under unbalanced grid conditions', *IEEE Trans. Ind. Electron.*, 2018, **66**, (3), pp. 2269–2279

[16] Yuan, Y., Zhao, C., Yuan, B., *et al.*: 'Analysis and optimization of reactive power controllers of voltage source converters in weak ac grid', *Power Syst. Technol.*, 2016, **40**, (3), pp. 696–703